Advanced Fiber Materials
https://doi.org/10.1007/s42765-024-00463-z

RESEARCH ARTICLE

Toughening and Responsive Contractile Shape Memory Fibrous Membrane via Water for Mechanically Active Wound Dressing

Wen Liu[1] · Wei Zhao[2] · Kunrong Xie[3] · Xue Feng Li[3] · Yufu Wang[3] · Deyan Kong[4] · Yanju Liu[2] · Jinsong Leng[1]

Received: 15 March 2024 / Accepted: 23 June 2024

Abstract

Conventional wound dressings only protect passively against bacterial infection. Emerging mechanically active adhesive dressings (AADs) are inspired by the active closure of embryonic wounds. It can promote wound healing by actively contracting the wound bed. AADs meet the requirements of high toughness, stimulus–response, and dynamic adhesion properties, which are challenging. Hence, we construct a water-responsive shape memory polyurea fibrous membrane (PU-fm) featuring favorable toughness, wet-adhesion, breathability, absorbency of four times its weight, and antibacterial. First, the water-toughened electrospun PU-fm is fabricated using a homemade polyurea (PU) elastomer with multistage hydrogen bond networks as a spinning solution. Furthermore, a Janus-structured polyurea-polydopamine-silver fibrous membrane (PU@PDA@Ag-fm) is engineered, integrating antibacterial properties without compromising mechanical robustness. It demonstrates strong adhesion to the skin, actively promotes wound contraction, and enables adaptive wrapping of tissues of varying sizes by the water-driven shape memory effect. Antibacterial tests and wound healing experiments indicate that the PU@PDA@Ag-fm has favorable antibacterial properties against *Escherichia coli* (*E.coli*) and accelerates the wound healing rate by 20%. For the first time, water-responsive shape memory PU-fm as the AADs is constructed, providing a new strategy for wound management. This can be extended to applications in other smart devices for biomedicine such as tendon repair, and bioelectronic interfaces.

Keywords Mechanically active dressing · Electrospun fibrous membrane · Janus structure · Water-responsive shape memory

1 Introduction

Bacterial infections will lead to delayed wound healing or even non-healing, seriously threatening life safety [1]. Wound dressings serve as a temporary protective layer, replacing compromised skin during the wound healing process. Wound dressings mitigate or prevent wound infection and facilitate an optimal environment for tissue regeneration and healing [2]. To further promote wound healing, biochemical function dressings with bioactive agents such as growth factors and cells, have been extensively studied, but some challenges such as complex manufacturing processes, uncontrolled drug release, and drug resistance, are difficult to overcome [3].

Wound healing is accompanied by an inward contraction of the wound bed, and the rate of wound contraction directly affects wound healing [4]. Embryonic healing exhibits a similar phenomenon that the contraction of cells around the wound pulls the edges of the wound together.

✉ Jinsong Leng
lengjs@hit.edu.cn

1 National Key Laboratory of Science and Technology On Advanced Composites in Special Environment, Harbin Institute of Technology, Harbin 150080, People's Republic of China

2 Department of Astronautical Science and Mechanics, Harbin Institute of Technology (HIT), No. 92 West Dazhi Street, P.O. Box 301, Harbin 150001, People's Republic of China

3 Department of Orthopedic Surgery, Second Affiliated Hospital of Harbin Medical University, No. 246, Baojian Road, Harbin 150086, People's Republic of China

4 MIIT Key Laboratory of Critical Materials Technology for New Energy Conversion and Storage, School of Chemistry and Chemical Engineering, Harbin Institute of Technology, No. 92, West Dazhi Street, Harbin 150001, People's Republic of China

Published online: 09 July 2024

Based on the theory, Blacklow et al. [5] first reported AADs that rely on the active contraction force to promote wound closure. The AADs must fulfill the following three requirements [4, 6–8]: high mechanical strength and stretchability, the ability to produce contraction force when stimulated, and strong adhesion that effectively transfers contractile forces to the underlying wound edges. However, it is difficult for dressings to meet these requirements simultaneously. A recent research about water-responsive contractile film can wrap nerves, muscles, and new organs of different sizes without sutures [9]. The shape memory heat-shrinkable tube can wrap the cables for protection [10]. However, the heat-driven shape memory polymer (SMP) is not suitable for human tissue [11], and water is a clean stimulation. What is more, the fresh wound surface contains a lot of water. Researchers have developed tunable, self-expanding, and drug-releasing functions of water-responsive SMP [12]. However, water-responsive SMP commonly faces complex programming, and prolonged recovery times [13]. Therefore, water-responsive SMP with fast response and controlled programming is highly desirable for biomedical applications.

Among all SMP, shape memory electrospun fibrous membrane is particularly appealing for biomedical applications due to their high porosity, and tunable micro- to nano-scale structures [14–18]. Besides, the nanofiber microstructure is similar to the natural extracellular matrix which is important for cell adhesion and growth [19, 20]. However, the traditional fibrous membrane exhibits poor tensile strength and stretchability due to the physical accumulation of nanofibers. The current shape memory fibrous membrane cannot satisfy the large deformation shrinkage and water-driven fast response.

Hence, we design a shape memory PU-fm featuring water-induced toughening and water-induced contraction to promote wound closure. PU-fm with hydrophilic groups can absorb water molecules so that the fibers form hydrogen bonds with water molecules, increasing the slip between the stacked fibers, and resulting in higher toughness. In addition, it can form immediately interfacial hydrogen bonds with the wet interface, ensuring strong wet adhesion that efficiently transfers contractile forces to wound edges. Besides, to endow PU-fm with physical antimicrobial properties without sacrificing mechanical strength and stretchability, a Janus structure is constructed to provide a platform for synergistic functional and mechanical properties. Further, water-induced shape contraction is demonstrated by closing the wound and wrapping the heart. Finally, antibacterial properties against *E. coli* and promote wound healing are demonstrated by antibacterial tests and wound healing experiments. To the best of our knowledge, this is the first combination of water-responsive shape memory electrospun PU-fm and AADs for wound management.

2 Experimental Section

2.1 Fabrication of PU Elastomer

The specific methodology was detailed in our previous work [21]. Briefly, dehydrated ED2000 was dissolved in DMAc, and then dropped into HMDI solution at room temperature stirring for 0.5 h. Further, a 7% mass fraction of the 1,3-Diamino-2-propanol solution was dropped into the above reaction system, keeping the reaction 24 h at room temperature. The viscous reaction solution was then cast into a mold and placed in a 60 °C drying oven to dry overnight. The preparation process and chemical structure were shown (Fig. S1).

2.2 Fabrication of PU-fm

The prepared PU elastomer was dissolved in a mixture of DMAc and CH_2Cl_2 (7:3) to form a transparent viscous 25% (mass fraction) electrospun solution. Then, a plastic syringe was linked in a rubber hose equipped with a metal nozzle connecting to the positive terminal of the high voltage power, and the negative terminal of power was connected to the collection roller locating 15 cm below the metal nozzle. Electrospinning parameters were ascertained including of temperature of (25 ± 2) °C and relative humidity of (35 ± 5)%, the syringe feed rate of 0.6 mL/h and a 15 kV of high voltage power.

2.3 Fabrication of PU@PDA-fm

The prepared PU-fm was immersed in a 2 mg/mL dopamine (DA) aqueous solution and the pH was adjusted to 8.5 using tris(hydroxymethyl)aminomethane (tris) buffer, stirring maintained for 24 h at room temperature. Subsequently, the membrane was rinsed with deionized water and dried, resulting in a distinct color transition from white to brownish-black.

2.4 Fabrication of PU@PDA@Ag-fm

$NH_3 \cdot H_2O$ was added drop by drop to 12 g/L or 6 g/L $AgNO_3$ solution until the solution changed from cloudy to clear, and the silver ammonia solution was prepared. Further, the PU@PDA-fm was soaked in silver ammonia solution stirring for 30 min. Next, 24 g/L or 12 g/L glucose solution was added drop by drop to silver ammonia solution with stirring intensely for 24 h. Finally, the prepared sample was washed with deionized water several times to wash away the unstable Ag nanoparticles on the surface.

A grayish-white membrane was obtained by drying oven at 30 °C.

3 Results and Discussion

3.1 Design and Fabrication of PU-fm and PU@PDA@Ag-fm

The mechanical property of electrospun fibrous membrane can be enhanced by improving the stack regularity of nanofibers and the mechanical property of electrospun polymer. Homemade humidity-responsive PU with high toughness is selected as the electrospun polymer [21, 22]. The molecular network of the electrospun solution is a reversible hydrogen bond network increasing segment slip to ensure the balance of strength and stretch-ability in Fig. 1a. Additionally, in Fig. 1b, a viscous electrospun solution is expelled from the needle nozzle and drawn into incredibly tiny fibers by an electrostatic filed, which cures quickly and creates fiber. As the accumulation of time increases, a pure white PU-fm is collected without spray powder, spray liquid, and granular feeling in Fig. 1c. The PU-fm (30 mm*10 mm*0.11 mm) can resist 400% strain without breaking, indicating favorable stretch-ability (Fig. S2). In addition to excellent stretch-ability, antibacterial properties are essential for medical materials. Ag is well known for its antimicrobial properties, and Ag atoms located on the surface of metallic Ag or Ag-covering materials can release free Ag^+ in the presence of H_2O and O_2 in the environment [23]. These Ag^+ are highly biologically active and have a strong killing effect on microorganisms such as bacteria and viruses [24]. However, Ag nanoparticles are easy to agglomerate and are usually encased in a matrix resulting in limited antimicrobial properties. PDA with strong non-selective adhesion properties and strong adsorb ability to $Ag(NH_3)_2^+$, provides firm sites for in situ growth of Ag nanoparticles [25]. To endow the PU-fm with antibacterial properties without

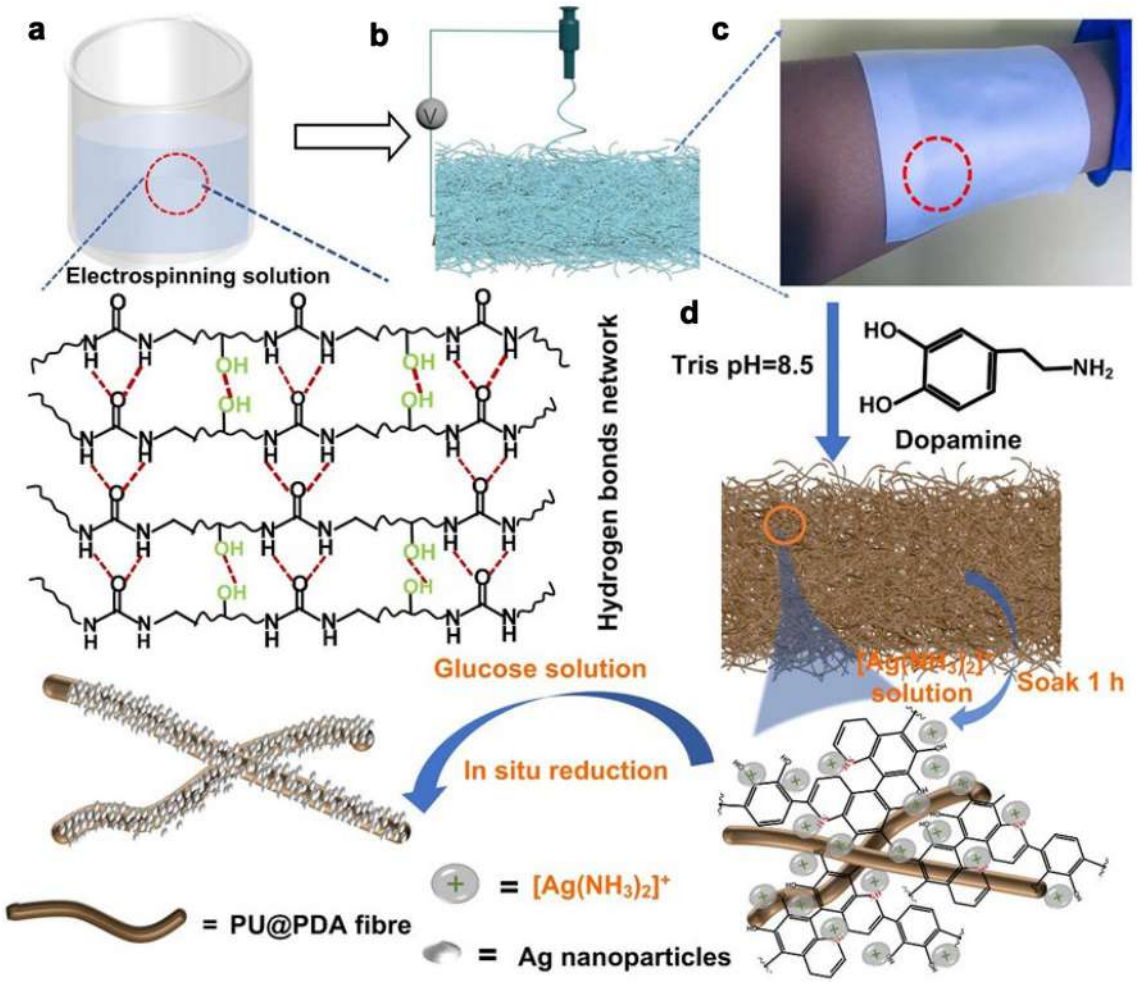

Fig. 1 Preparation and structure of PU-fm and PU@PDA@Ag-fm. **a** Molecular structure of electrospun solution. **b** Collection process of PU-fm. **c** Actual image of the collected PU-fm. **d** Schematic fabrication process of PU@PDA@Ag-fm

sacrificing mechanical properties, PU@PDA@Ag-fm is constructed with a Janus structure integrating the targeting of Ag bacteria with the photothermal properties of PDA in Fig. 1d. The prepared PU-fm is immersed in dopamine (DA) solution, and DA spontaneously polymerize on the nanofibers forming PDA. The -OH and -NH_2 groups on the PDA surface can adsorb $Ag(NH_3)_2^+$ to the nanofibers surface, and $Ag(NH_3)_2^+$ is reduced to Ag nanoparticles and grows tightly on the nanofibers wall forming a stable Janus structure. The deposition amount of Ag can be adjusted by controlling the concentration of $AgNO_3$ solution. Therefore, combining the favorable toughness of PU-fm and the photo-thermal bacterial property of PDA, an advanced PU@PDA@Ag-fm dressing is fabricated.

3.2 Structural and Mechanical Property of PU-fm, and PU@PDA@Ag-fm

To confirm micro-morphology structure and composition, scanning electron microscopy (SEM) and energy dispersive spectroscopy (EDS) are employed. Excellent spinning quality contributes to improving the mechanical property. The spinning quality can be measured by SEM. Nanofibers have smooth surfaces, and with uniform size in Fig. 2a, corresponding EDS image in Fig. S3a. Compared with Fig. 2a, Fig. 2d shows that each nanofiber is covered with nanoparticles corresponding EDS image (Fig. S3b), and only a few scattered particles is caused by the excessive load of Ag under 12 g/L $AgNO_3$ solution. Notably, the scattered Ag nanoparticles are clustered together, while the Ag deposited on the fiber wall is uniformly dispersed because of the strong attraction of the PDA for $Ag(NH_3)^{2+}$ to improve the dispersion of Ag nanoparticles. The nanoparticles all grow on the nanofiber wall at a concentration of 6 g/L of $AgNO_3$ solution (Fig. S4), suggesting an adjustable Ag deposition amount. Average fiber diameters (d_{av}) are measured and fitted to calculate the thickness of nanoparticles. d_{av} of PU fiber is 1.34 μm in Fig. 2b and d_{av} of PU@PDA@Ag fiber increases to 1.88 μm in Fig. 2e, suggesting that the deposition thickness of Ag nanoparticles is 0.27 μm. Ag deposition doesn't increase the RMS roughness (Rq) of PU-fm in Fig. 2c, 2f, indicating that the interlayers of the fibrous membrane are denser due to the in situ growth of Ag. The PU@PDA@Ag-fm contains 67% (mass fraction) Ag (Fig. S3c), and its EDS with different element colors are shown in Fig. 2g. As shown in Fig. 2g1, Ag is uniformly covered without aggregation, because the color uniformity on the fiber wall is consistent with the C and O elements in Fig. 2g2 and g3. PU and PU@PDA present a bread peak at $2\theta = 18.8°$, a typical amorphous structure in Fig. 2h. For PU@PDA@Ag-fm, the diffraction peaks of metallic Ag are observed at 38.3°(111), 44.4°(200), 64.6°(220), 77.6°(311), 81.7°(222), confirming that the nanoparticles is Ag rather than AgO. The Ag nanoparticles belong to antibacterial activity face-centered cubic crystal structure [26, 27]. The physical and chemical interactions between PU, PDA, and Ag is confirmed by FTIR spectra (Fig. S5). For the PU spectrum, the free C = O peak is matched in 1 740 cm^{-1}, and the C-H peak is matched in 722 cm^{-1}. Compared with PU@PDA spectra, two peaks disappear to form intermolecular hydrogen bonds between PU and PDA. Compared with PU, a new peak corresponding to Ag3d appears in the PU@PDA@Ag (Fig. S6a). The characteristic peaks at 373.5 eV and 367.5 eV correspond to Ag3d5/2 and Ag3d3/2 of Ag0, respectively, indicating that Ag nano-particles have been effectively assembled on the surface of PU@PDA (Fig. S6b).

Favorable spinning effect and uniform particle deposition provide the basis for mechanical properties. Predictably, in Fig. 2j, stress increases from 8.6 to 10.7 MPa, and strain increases from 457 to 522%, because the density between layers is improved by the bonding PDA and deposition Ag nanoparticles resulting in increased mechanical properties. The introduction of functionality does not lead to a deterioration in mechanical properties, but to enhancement, because the Janus structure provides a compatible platform for functionality and mechanical properties [28]. Finally, PU-fm or PU@PDA@Ag-fm are far superior to many recently reported electrospun fibrous membranes in strength and stretchability, and exhibit the highest toughness in Fig. 2k [29–35], which enhances the stimulus-responsive strain shrink.

3.3 Effect of Water on Microstructure and Mechanical Property

3.3.1 Water Absorbency

The dressings' breathability and hydrophilic properties ensure unobstructed airflow around the wound while efficiently absorbing exudates and secreted perspiration. This facilitates the drainage of purulent discharge from the body to promote wound healing. The hydrophilicity is characterized in Fig. 3a. The contact angle changes from 114° to 0° in 11 s indicating super-hydrophilicity of PU-fm. PU@PDA-fm has the fastest liquid absorption capability, with the contact angle decreasing from 109° to 0° in just 5 s in Fig. 3b and Fig. S7. This is because of the abundance of hydrophilic groups, such as -OH and -NH_2 in PU@PDA-fm. The contact angle of PU@PDA@Ag-fm decreases from 105° to 0° in 35 s due to deposition of Ag, but it is still super-hydrophilic. Absorbency is characterized by testing its water absorption since blood is made up of 90% water. Each gram of PU-fm absorbs four times water only 4 s arriving stability in Fig. 3c, suggesting that only 0.125 g PU-fm absorbs 500 mL of exudate. As shown in Fig. 3d, the PU-fm's breathability is

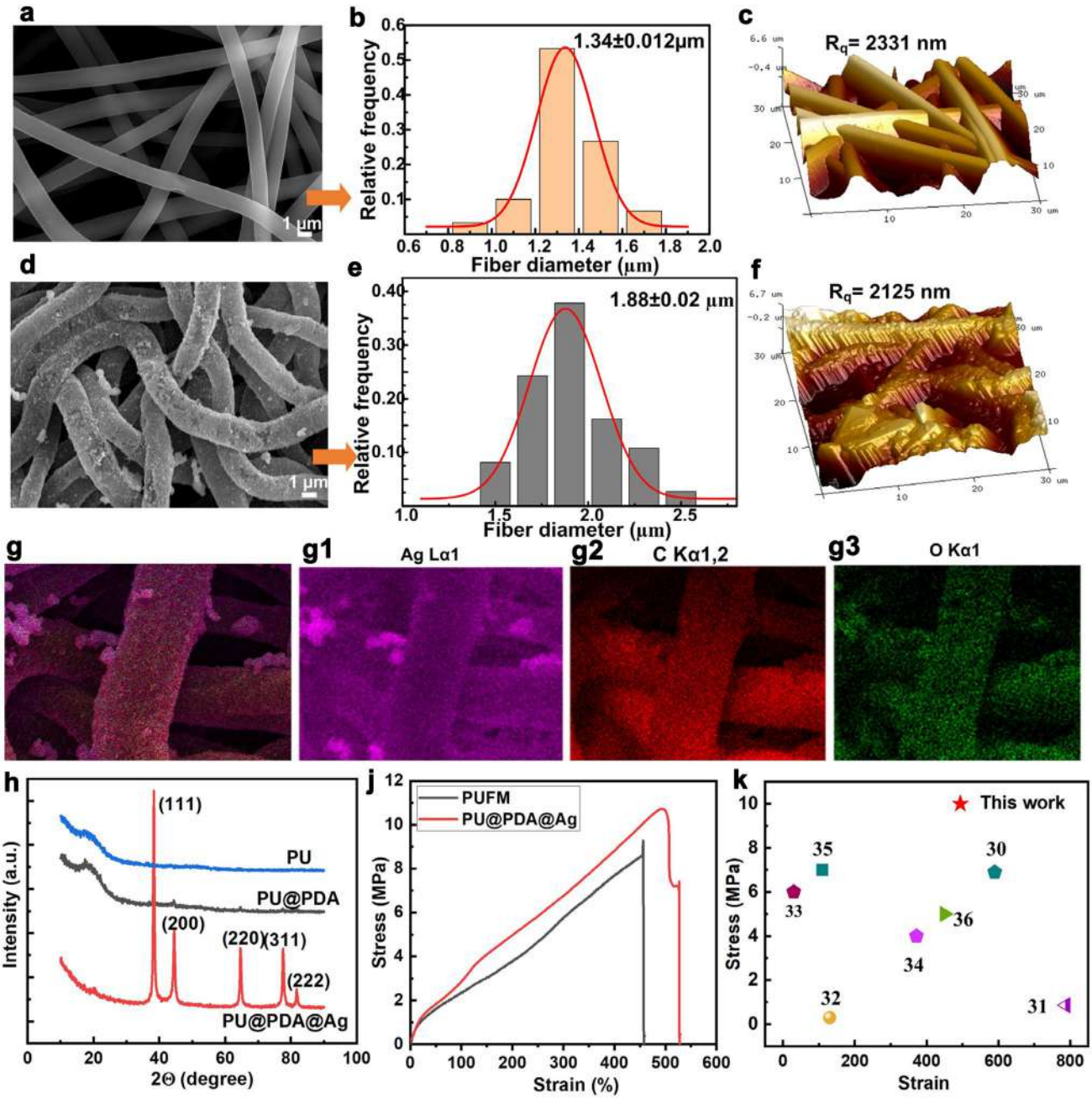

Fig. 2 Micro-structure of PU-fm and PU@PDA@Ag-fm. SEM image of **a** PU-fm, and **d** PU@PDA@Ag-fm. The average diameters of **b** PU-fm, and **e** PU@PDA@Ag-fm. Surface roughness of **c** PU-fm, and **f** PU@PDA@Ag-fm. **g**–**g**3 EDS image of different elements of PU@PDA@Ag-fm. **h** XRD spectrum. **j** Strain–stress plot of PU-fm, and PU@PDA@Ag-fm. **k** Comparison of mechanical properties of the reported electrospun fibrous membrane

demonstrated by a water vapor condensation experiment. Water vapor quickly passes through the PU-fm and condenses into droplets at the bottom of a beaker, reflecting the breathability.

3.3.2 Microstructure Change

To more intuitively illustrate the effect of water on the structure, the microstructure of dry and wet states is

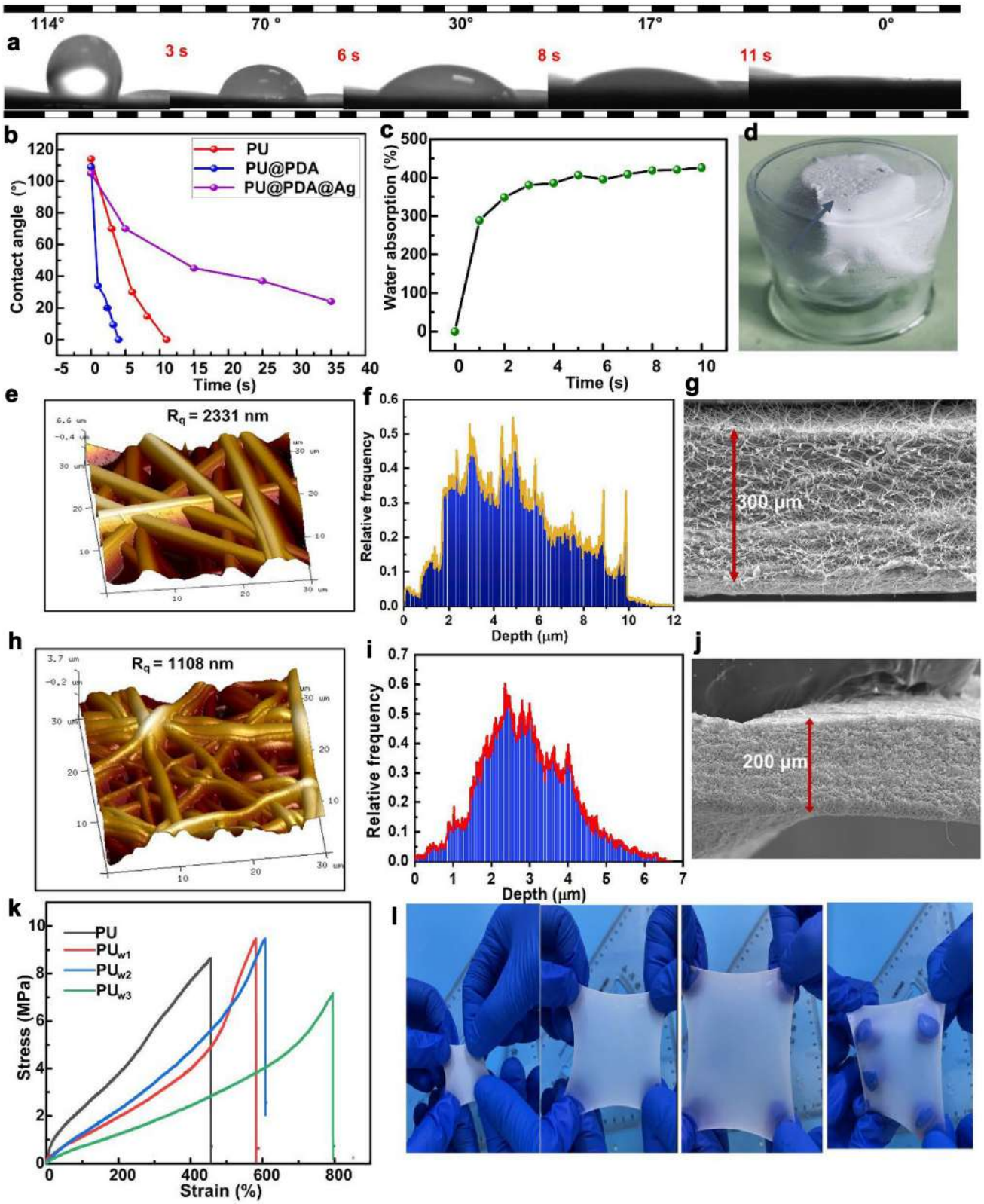

Fig. 3 The structural and mechanical properties of PU-fm respond to water. **a** Hydrophilicity of fibrous membrane. **b** Contact angle changes with time. **c** Water absorption of PU-fm. **d** Breathability of PU-fm. **e** RMS roughness of dry PU-fm. **f** Surface evenness of dry PU-fm. **g** Section SEM images of dry PU-fm. **h** RMS roughness of wet PU-fm. **i** Surface evenness of wet PU-fm. **j** Section SEM images of wet PU-fm. **k** Stress–strain plot of PU-fm after soaking at different times in water. **l** Demonstration of a biaxially stretched wet PU-fm

characterized. The R_q of dry PU-fm is 2331 nm in Fig. 3e, but the R_q of wet PU-fm is 1108 nm in Fig. 3h, indicating that wet PU-fm has a more irregular surface. Further, surface roughness distribution of dry PU-fm is wide, and it is mainly divided into 2–8 μm in Fig. 3f, and the wet PU-fm is concentrated on 2–4 μm in Fig. 3i, indicating more uniform interlayer structure. By comparing the SEM image of a cross-section, the thickness of dry PU-fm is about 300 μm and the gap between layers is large and messy in Fig. 3g. However, the wet PU-fm is more orderly, and the thickness is reduced to 200 μm and the stack is more compact in Fig. 3j. This is very beneficial for tightening wound, avoiding the problem of wet-adhesive hydrogels expanding and peeling the wound in wet environment [36].

3.3.3 Mechanical Property Change

Structure changes directly affect the mechanical properties. According to different soaking times in the water, PU-fm is named as PU, PU_{w1}, PU_{w2}, and PU_{w3} to study the effect of water on tensile property. The PU-fm has different stress–strain shapes in wet and dry states in Fig. 3k. The stress–strain plot suggests that PU is a typically strong and hard material, and the tensile strength reaches 8.6 MPa corresponding to 457% strain. Different from the PU plot shape, stress–strain plots of PU_{w1}, PU_{w2}, and PU_{w3} are subjected to a small stress accompanied by a big strain. Until it breaks, the stress sharply rises, which is a typical soft and tough material. Concretely, the tensile strength and elongation at break of $PU_{w1}$and PU_{w2} increase to 9.3 MPa, 9.4 MPa, and 579%, 604%, which is higher than PU. For PU, -OH groups in the side chains and the urea bonds in PU main chains form intermolecular hydrogen bonds. However, there are large gaps between the layers with poor molecular slip (Fig. 3g). When water molecules enter interlayers of PU-fm, the hydrogen bonds between PU molecules are slightly opened and re-established between water molecules and PU. The water molecules act as bound rather than free water between the layers and increase the interlayer slipperiness of PU-fm. The PU_{W3} strain increases to 793%, and tensile strength decreases to 7 MPa. As the soaking time increases, PU-fm becomes saturated. A large amount of water enters the interlayer, destroying the ordered hydrogen bond structure and causing hydrogen bond dissociation, which greatly reduces the tensile strength of PU-fm and increases the ductility [37, 38]. For the dry and wet states of PU-fm, hanging the same 200 g weight produces a deformation difference, indicating that the wet PU-fm becomes softer but has better elastic recovery (Fig. S8a). In Fig. 3l, a wet PU-fm (3 cm × 3 cm) is stretched into a transparent membrane with an increased area of about 9 cm× 9 cm. This is nearly a nine-fold increase indicating excellent toughness (Movie S1). Just like the silk reeling process of a cocoon, a pliable silk pocket is formed (Fig. S8b). Hence, the unique water molecule zipper structure increases the toughness of PU-fm, which provides a basis for high contractility.

3.3.4 Water-Driven Shape Memory Mechanism

The composition of tissue fluid in the biological body is mainly water, so it is very meaningful to develop a soft membrane being stimulated by water in a biological therapy system [9]. Different from conventional heat-driven SMP depending on the reversible and stationary phases of the molecular network [39], the water-driven shape memory PU-fm is based on the recombination of reversible hydrogen bonds network [40]. Figure 4a shows the temporary shape programming process by water, and corresponding molecular structural changes are presented in Fig. 4(i–iii). Minutely, PU-fm is fixed in different shape molds after absorbing water. As the water naturally evaporates, temporary shapes are obtained, such as hat-shaped, spiral (Fig. S9). The mechanism of the shape memory effect by water-driven is explained by molecular structure changes: i. The chain segment of the original shape is the lowest energy state with a large number of hydrogen bonds. ii. Water molecules are absorbed within the molecule structure, breaking the original hydrogen bond arrays to reform new hydrogen bond arrays. iii. After the water evaporates, hydrogen bonds are reorganized to form new hydrogen bond arrays contributing to a temporary shape. iv. When PU-fm touches a wet surface again, the intermolecular hydrogen bonds with the unilateral water molecule pull the membrane to unfold. The curled fibrous membrane recovers to a flat state covering the water in Fig. 4b. Vividly, a schematic diagram of forces acting at two interfaces is presented in Fig. 4c, and the force is a kind of hydrogen bonds attraction in water molecules and PU-fm.

3.3.5 Demonstration Model of Water-Induced Shrink

Traditional dressing such as cotton and gauze, adheres to a new granulation tissue during the healing process, causing pain and tear when it is removed. As a physiologically regulated adhesive wound dressing, wet adhesion is formed by forming intermolecular hydrogen bonds with the wound interface and is capable of avoiding secondary injury of the wound [36]. Predictably, the PU-fm well adheres to the irregular wound surface in Fig. 5a. The PU-fm is tightly attached to the surface of the wound in Fig. 5b (Movie S3), which efficiently transfers contractile forces to the underlying wound edges. The PU-fm is closely fitted to cover the wound, which is inseparable from its low modulus and silkiness. As shown in Fig. 5c, the wet-adhesive mechanism is that a large number of -OH groups of PU-fm side chains form hydrogen bonds with water molecules in the blood. The wet-adhesive effect can increase the tightness and fit between

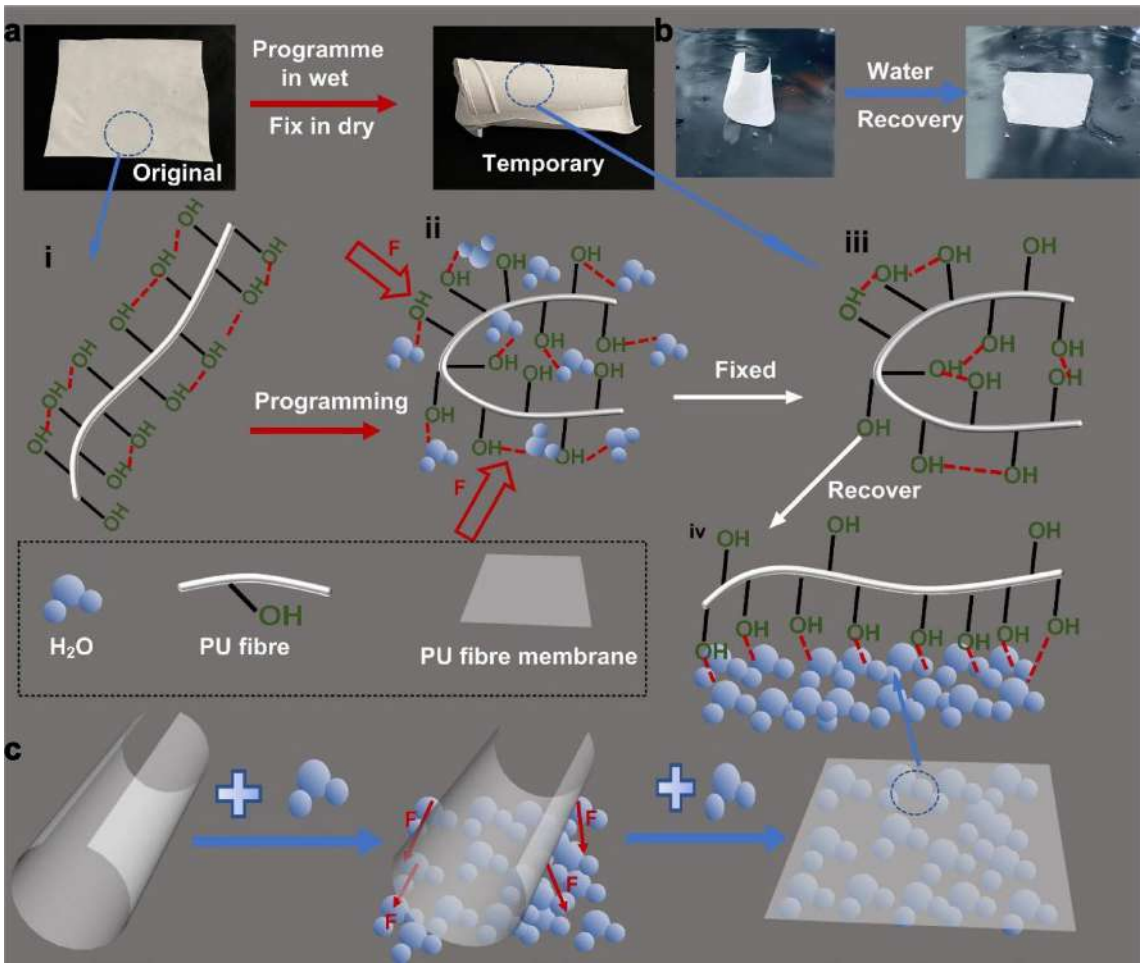

Fig. 4 Water-driven shape memory mechanism. **a** Programming process of PU-fm from an unfolded state to a curled state (i–iii Change diagram of corresponding molecular structure). **b** Water-driven shape recovery process. **c** Water-driven recovery schematic (iv Change diagram of corresponding molecular structure)

a dressing and a wound [7]. PU-fm is tightly attached to the wet skin, when the moisture on the skin surface is dry, the PU-fm automatically falls off (Fig. S10), which explains its physiologically regulated adhesive property. Wet adhesion is a basic requirement for mechanically active dressings, while responsive contraction is essential for wound closure.

Next, based on the water-responsive shape memory effect of PU@PDA@Ag-fm, two application models are demonstrated. The first model is an external wound model in Fig. 5d, the pre-stretched 50% PU@PDA@Ag-fm is wrapped directly around the wet wound and it adheres to the tissue without any fixation by its wet adhesion character. The pre-stretched PU@PDA@Ag-fm generates a contraction force in the shape recovery process to promote wound closure in Fig. 5dii. A 10 mm wide wound is closed in Fig. 5di, and the separated wound is rejoined in Fig. 5diii. Different from nonantibiotic bactericides [41, 42], PU@PDA@Ag-fm is a physical method that water-driven shape recovery promoted actively wound closure (Movie S4). As shown in Fig. 5e, when the temporary shape is 50%, 100%, 150%, and 200% strain, respectively, the corresponding R_r is a decreasing trend. For example, when the temporary shape is 50% and 100% strain, R_r reaches 100%. However, when the temporary shape is 150% and 200% strain, R_r decreases to 85% and 70%, respectively. Because the shape recovery force of PU@PDA@Ag-fm is produced by the hydrogen bond rearrangements under a water-driven molecular network, the excessive molecular gap causes the hydrogen bonds to be unable to rebond affecting its shape recovery rate (R_r).

As shown in Fig. 5f, a fixed-shape ring with a diameter of 20 mm is set on a plastic pipe with a diameter of 10 mm, and it can shrink and tightly wrap on the wall within 12 s by water (Movie S5). This process is like the earliest shape memory heat shrink tubing. It can shrink to protect the circuit and devices [10]. The heat shrink tube is driven by a high temperature and is suitable for the engineering field. The PU@PDA@Ag-fm is driven by green water, which is very convenient in the tissue. What is more, PU@PDA@

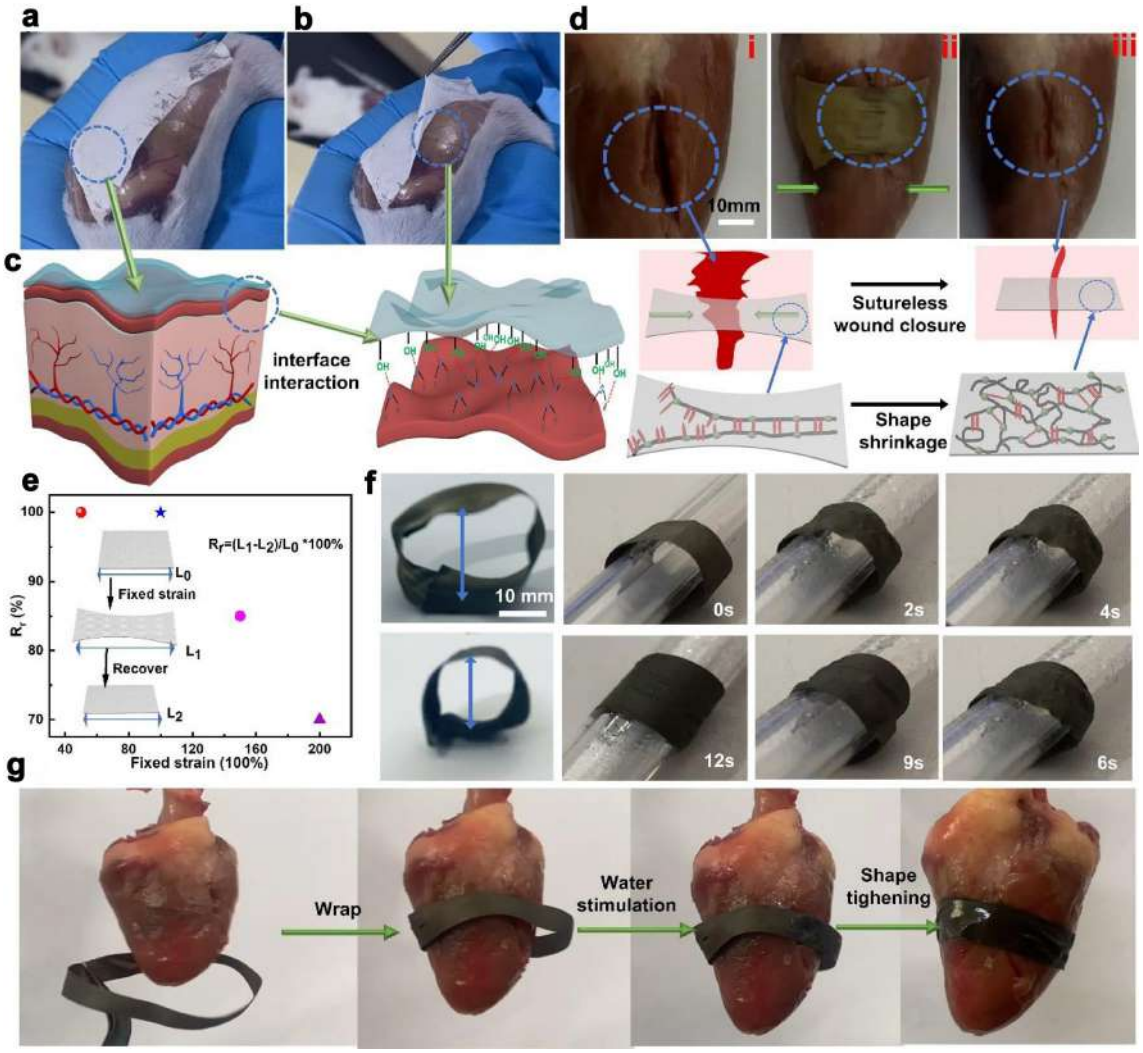

Fig. 5 Application model based on the shape shrinking. **a**-**b** Wet-adhesion to wet wounds. **c** Schematic diagram of wet-adhesion. **d** Concept demonstration of PU@PDA@Ag-fm for wound closure and changes of molecular structure in the process. **e** The effect of strain on R_r. **f** Shape shrink-wrapped a plastic pipe. **g** Application concept of water-driven shrink-wrapped heart

Ag-fm has a faster water response compared with previous report with 7 h responsive recovery [13]. As shown in Fig. 5g, the 40 mm diameter PU@PDA@Ag-fm shrinks rapidly under water drive and wraps the heart without sutures, serving as a bioelectronic interface to monitor and treat heart disease. The water-driven shrinkable PU@PDA@Ag-fm is promising in electronic biological interfaces as well as mechanically active dressings [9].

3.4 The Photo-Thermal Effect and Antimicrobial Property of PU@PDA@Ag-fm

When human skin is broken, pathogenic microorganisms enter the body through small wounds causing infections and diseases. AADs promote wound closure, but cannot kill the bacteria. The photo-thermal effect can promote local microcirculatory blood flow, inhibit bacteria, and reduce inflammation [43]. The photo-thermal effect of the PU@PDA-fm is evaluated by an 808 nm near-infrared (NIR) laser with different intensities. Specifically, the PU@PDA-fm temperature increases from 25 to 50 °C only 75 s under the NIR laser (5 mW/cm^2) in Fig. 6(a, b). Under 15 mW/cm^2 NIR laser irradiation, the temperature increases from 25 to 100 °C. Compared with PU@PDA@Ag-fm in Fig. 6(c, d), the coating of Ag results in a lower photo-thermal effect than PU@PDA under 5 mW/cm^2 irradiation. Owing to the strong penetrating power of NIR, the PU@PDA@Ag-fm can effectively convert NIR light energy into heating under 10 and 15 mW/cm^2. The PU@PDA@Ag-fm surface arrives at 50 °C under 10 mW/cm^2 and arrives at 105 °C under 15 mW/cm^2.

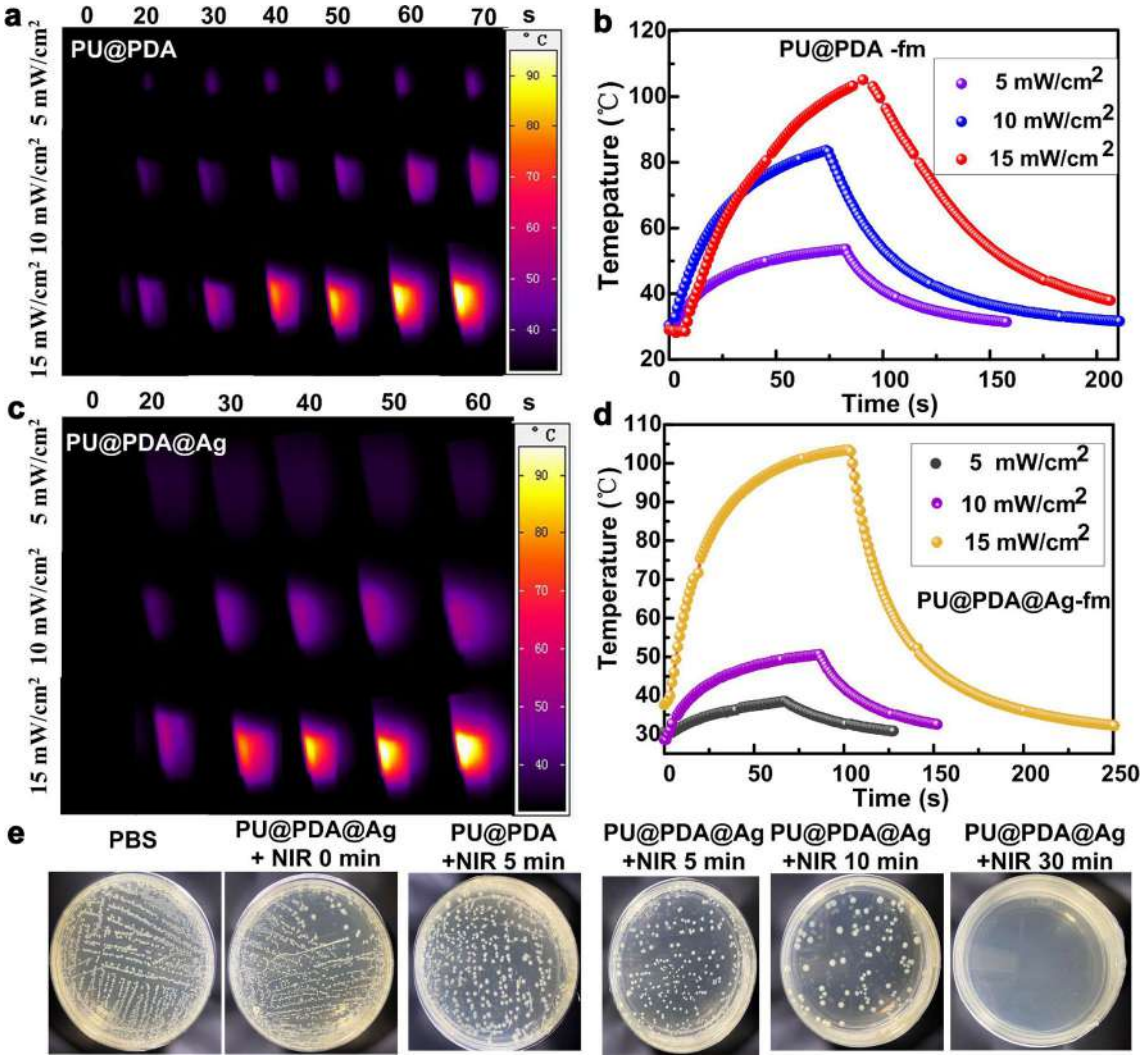

Fig. 6 Photo-thermal and antibacterial properties of fibrous membranes. **a** NIR thermal images and **b** Photo-thermal temperature plots of PU@PDA-fm under diverse NIR laser intensity (5, 10, and 15 mW/cm^2). **c** NIR thermal images and **d** Photo-thermal temperature plots of PU@PDA@Ag-fm under diverse NIR laser intensity (5, 10, and 15 mW/cm^2). **e** Bacterial colony of *E.coli* after different treatments

High temperatures can damage normal tissue, so a laser intensity of 10 mW/cm^2 is selected to test antibacterial properties.

To evaluate the antibacterial properties of PU@PDA@Ag-fm, Gram-negative *E.coli* is chosen as a research object because of a common bacteria in infected wounds [44]. Compared with the control group, colonies of PU@PDA@Ag + NIR-0 min group have a decreasing trend in Fig. 6e, because PU@PDA@Ag-fm releases Ag^+ to inhibit bacterial growth [27]. After irradiating for 5 min, the colonies of PU@PDA@Ag + NIR-5 min are reduced, compared with PU@PDA + NIR-5 min, indicating PU@PDA@Ag with better antimicrobial property. The excellent antibacterial property of PU@PDA@Ag is mainly attributed to the NIR-induced photo-thermal effect of PDA and the release of Ag^+. When irradiation time lasts 30 min, *E. coli* almost all are killed. Effective bacterial ablation can avoid wound infection and promote wound healing. Finally, because of the uniform and stable deposition of Ag nanoparticles, PU@PDA@Ag with excellent electrical conductivity is discussed in Fig. S11 and Fig. S12, which offers a possibility for electronic biological interfaces. Almost all cells have a strong green signal and normal spindle-like morphology by Toxicity test (Fig. S13), suggesting PU@PDA@Ag-fm's non-toxicity.

3.5 Wound Healing of PU@PDA@Ag-fm

Further, the contribution of PU@PDA@Ag-fm on wound tissue regeneration is estimated by constructing a skin defect model [45]. The building process is shown in Fig. 7a. Wound

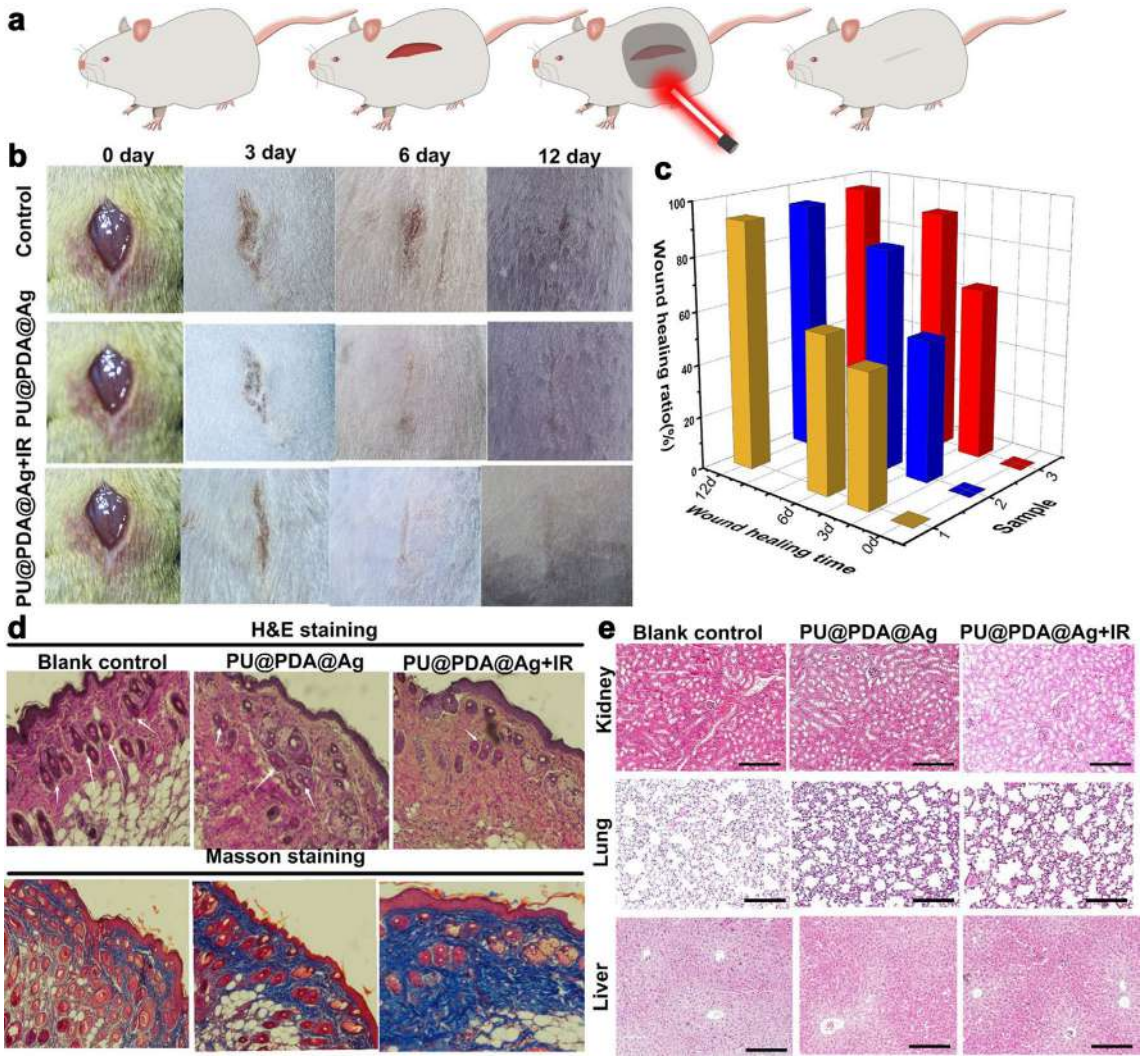

Fig. 7 Promoting wound healing of the PU@PDA@Ag-fm. **a** Schematic of acting on mouse wounds. **b** Digital photographs of wound healing at 0, 3, 6, and 12 days for different groups. **c** Wound healing ratios for different groups. **d** Corresponding H&E and Masson staining sections of healing 3 days. **e** Optical microscope H&E staining images of visceral tissue (kidney, lung, and liver) for healing 12 days. The scale bar is 100 μm

healing images of three groups are shown in Fig. 7b under healing on different days. The wound healing ratio is calculated in Fig. 7c. For undergoing 3 days of healing treatment, the wound healing ratio of the PU@PDA@Ag + IR group reaches 65%, the PU@PDA@Ag group is 53%, and the control group is 45%. PU@PDA@Ag + IR group has the best healing effect because the photo-thermal effect and Ag^+ release prevent wound infection and promote wound tissue metabolism to accelerate wound healing [46]. With healing lasting 12 days, the wound healing ratio reaches 96%, 93%, and 90%, respectively, without significant difference. The first 3 days after trauma is a critical period, because it involves a phase of inflammatory response that directly affects tissue proliferation, granulation, and the restoration of skin continuity [47].

The H&E and Masson staining of histopathological skin wounds are employed to assess trauma issues [48], and tissue slice data of different experiment groups are demonstrated (Fig. 7d). After comparing, an obvious feature of the PU@PDA@Ag + IR group is fewer inflammatory cells marked white arrow and thicker granulation tissue. Further, collagen deposition, a vital indicator of wound healing, is dyed blue by Masson staining distinguishing a visible relative intensity change representing indicative of collagenous fiber [49]. Compared with other two groups, the PU@PDA@Ag + IR group has the most pronounced collagen fiber deposition, which accelerates the wound healing. To study the toxicity of the PU@PDA@Ag-fm over wound sites to internal organs, histological analysis of the mice about kidney, lung, and liver is demonstrated (Fig. 7e). Compared

with the control group, the organ structure of the mice is not obvious cell necrosis, inflammatory lesions and organ injury. PU@PDA@Ag-fm with excellent biocompatibility and high biosafety is capable of promoting wound healing.

4 Conclusions

In summary, water-responsive PU@PDA@Ag-fm with photo-thermal bactericidal property are fabricated by a combination of electrospun technique and Janus structure. Based on humidity responsive PU elastomer as spinning fluid, PU-fm with the tensile strength of 8.6 MPa corresponding to a strain of 457% is prepared. The PU-fm absorbs 4 times its own mass of water, indicating favourable water absorbency. After absorbing water, the PU-fm area can increase by 9 times when biaxially stretched. PU-fm with favorable toughness, wet adhesion and water-driven shape memory effect meets the requirements for toughness, stimulation response, and adhesion of AADs. By in-situ deposition of Ag nanoparticles on PU-fm wall, PU@PDA@Ag-fm with water-responsive contraction and wet adhesion, and the tensile strength is increased to 10.7 MPa. PU@PDA@Ag-fm can shrink to close a wound of 10 mm wide without sutures. A diameter of 40 mm annular PU@PDA@Ag-fm contracts to 20 mm and wraps around a heart within seconds under water stimulation. Through the experiments of *E.coli* sterilization and wound healing, PU@PDA@Ag-fm has excellent antibacterial property resulting in a 20% increase in wound healing rate. Consequently, PU@PDA@Ag-fm holds considerable promise for broadened application prospects in various biomedical smart devices, including tendon repair and bioelectronic interfaces.

Supplementary Information The online version contains supplementary material available at https://doi.org/10.1007/s42765-024-00463-z.

Acknowledgements This research was supported by the National Key R&D Program of China (No. 2022YFB3805700), National Natural Science Foundation of China (No.92271206).

Declarations

Conflict of Interest The authors declare that they have no conflict of interest.

References

1. Ding Y, Liu X, Chen C. Global, Regional, and national trends in osteoarthritis disability-adjusted life years (DALYs) from 1990 to 2019: a comprehensive analysis of the global burden of disease study. *Public Health*. **2024**;*226*:261.
2. Luo R, Liang Y, Yang J, Feng H, Chen Y, Jiang X, Zhang Z, Liu J, Bai Y, Xue J, Chao S, Xi Y, Liu X, Wang E, Luo D, Li Z, Zhang J. Reshaping the endogenous electric field to boost wound repair via electrogenerative dressing. *Adv Mater*. **2023**;*35*:2208395.
3. Min Y, Han R, Li G, Wang X, Chen S, Xie M, Zhao Z. The pH-sensitive optical fiber integrated CMCS-PA@Fe hydrogels for photothermaltherapy and real-time monitoring of infected wounds. *Adv Funct Mater*. **2023**;*33*:2212803.
4. Chang L, Du H, Xu F, Xu C, Liu H. Hydrogel-enabled mechanically active wound dressings. *Trends Biotechnol*. **2024**;*42*:31.
5. Peng X, Dong K, Ye CY, Jiang Y, Zhai SY, Cheng RW, Liu D, Gao XP, Wang J, Wang ZL. A breathable, biodegradable, antibacterial, and self-powered electronic skin based on all-nanofiber triboelectric nanogenerators. *Sci Adv*. **2020**;*6*:eaba9624.
6. Cai C, Zhu H, Chen Y, Guo Y, Yang Z, Li H, Liu H. Mechanoactive nanocomposite hydrogel to accelerate wound repair in movable parts. *ACS Nano*. **2022**;*16*:20044.
7. Wang Z, Wan X, Wang S. Bioinspired chemical design to control interfacial wet adhesion. *Chem*. **2023**;*9*:771.
8. Hu J, Wei T, Zhao H, Chen M, Tan Y, Ji Z, Shen J, Han Y, Yang N, Chen L, Xiao Z, Zhang H, Liu Z, Chen Q. Mechanically active adhesive and immune regulative dressings for wound closure. *Matter*. **2021**;*4*:2985.
9. Yi J, Zou G, Huang J, Ren X, Tian Q, Yu Q, Wang P, Yuan Y, Tang W, Wang C, Liang L, Cao Z, Li Y, Yu M, Jiang Y, Zhang F, Yang X, Li W, Wang X, Luo Y, Loh XJ, Li G, Hu B, Liu Z, Gao H, Chen X. Water-responsive supercontractile polymer films for bioelectronic interfaces. *Nature*. **2023**;*624*:295.
10. Kong D, Xiao X. Rigid high temperature heat-shrinkable polyimide tubes with functionality as reducer couplings. *Sci Rep*. **2017**;*7*:44936.
11. Ni C, Chen D, Yin Y, Wen X, Chen X, Yang C, Chen G, Sun Z, Wen J, Jiao Y, Wang C, Wang N, Kong X, Deng S, Shen Y, Xiao R, Jin X, Li J, Kong X, Zhao Q, Xie T. Shape memory polymer with programmable recovery onset. *Nature*. **2023**;*622*:748.
12. Liang R, Yu H, Wang L, Amin BU, Wang N, Fu J, Xing Y, Shen D, Ni Z. Triple and two-way reversible shape memory polymer networks with body temperature and water responsiveness. *Chem Mater*. **2021**;*33*:1190.
13. Xie Y, Lei D, Wang S, Liu Z, Sun L, Zhang J, Qing FL, He C, You Z. A biocompatible, biodegradable, and functionalizable copolyester and tts application in water-responsive shape memory scaffold. *ACS Biomater Sci Eng*. **2019**;*5*:1668.
14. Dong R, Li Y, Chen M, Xiao P, Wu Y, Zhou K, Zhao Z, Tang BZ. In situ electrospinning of aggregation-induced emission nanofibrous dressing for wound healing. *Small Methods*. **2022**;*6*:2101247.
15. Liu XF, Zhang J, Liu JJ, Zhou QH, Liu ZQ, Hu PY, Yuan Z, Ramakrishna S, Yang DP, Long YZ. Bifunctional CuS composite nanofibers via in situ electrospinning for outdoor rapid hemostasis and simultaneous ablating superbug. *Chem Eng J*. **2020**;*401*:126096.
16. Si Y, Zhang Z, Wu WR, Fu QX, Huang K, Nitin N, Ding B, Sun G. Daylight-driven rechargeable antibacterial and antiviral nanofibrous membranes for bioprotective applications. *Sci Adv*. **2018**;*4*:eaar5931.
17. Yang G, Li X, He Y, Ma J, Ni G, Zhou S. From nano to micro to macro: electrospun hierarchically structured polymeric fibers for biomedical applications. *Prog Polym Sci*. **2018**;*81*:80.
18. Yan T, Wu Y, Tang J, Pan Z. Flexible strain sensors fabricated using aligned carbon nanofiber membranes with cross-stacked structure for extensive applications. *Int J Smart and Nano Mater*. **2022**;*13*:432.
19. Miguel SP, Sequeira RS, Moreira AF, Cabral CSD, Mendonça AG, Ferreira P, Correia IJ. An overview of electrospun membranes loaded with bioactive molecules for improving the wound healing process. *Eur J Pharm Biopharm*. **2019**;*139*:1.

20. Chen Y, Dong X, Shafiq M, Myles G, Radacsi N, Mo X. Recent advancements on three-dimensional electrospun nanofiber scaffolds for tissue engineering. *Adv Fiber Mater*. **2022**;*4*:959.
21. Liu W, He Y, Leng J. Humidity-responsive shape memory polyurea with a high energy output based on reversible cross-linked networks. *ACS Appl Mater Interfaces*. **2022**;*15*:2163.
22. Liu W, He Y, Leng J. Shape memory supramolecular polyurea with adjustable toughness and ultrahigh energy density. *ACS Appl Poly Mater*. **2022**;*4*:6092.
23. Zong D, Zhang X, Yin X, Wang F, Yu J, Zhang S, Ding B. Electrospun fibrous sponges: principle, fabrication, and applications. *Adv Fiber Mater*. **2022**;*4*:1434.
24. Gupta A, Maymes M, Silver S. Effects of halides on plasmid-mediated silver resistance in escherichia coli. *App Environ Microbiol*. **1998**;*64*:5042.
25. Wang Z, Wang W, Wamsley M, Zhang D, Wang H. Colloidal polydopamine beads: a photothermally active support for noble metal nanocatalysts. *ACS Appl Mater Interfaces*. **2022**;*14*:17560.
26. Qi X, Huang Y, You S, Xiang Y, Cai E, Mao R, Pan W, Tong X, Dong W, Ye F, Shen J. Engineering robust Ag-decorated polydopamine nano-photothermal platforms to combat bacterial infection and prompt wound healing. *Adv Sci*. **2022**;*9*:2106015.
27. Qie X, Zan M, Gui P, Chen H, Wang J, Lin K, Mei Q, Ge M, Zhang Z, Tang Y, Dong WF, Song Y. Design, synthesis, and application of carbon dots with synergistic antibacterial activity. *Front Bioeng Biotechnol*. **2022**;*10*:894100.
28. Sheng W, Li W, Yu B, Li B, Jordan R, Jia X, Zhou F. Mussel-inspired two-dimensional freestanding alkyl-polydopamine janus nanosheets. *Angew Chem Int Ed*. **2019**;*58*:12018.
29. Chen Q, Wu J, Liu Y, Li Y, Zhang C, Qi W, Yeung KWK, Wong TM, Zhao X, Pan H. Electrospun chitosan/PVA/bioglass Nanofibrous membrane with spatially designed structure for accelerating chronic wound healing. *Mater Sci Eng C*. **2019**;*105*: 110083.
30. Dong J, Peng Y, Nie X, Li L, Zhang C, Lai F, He G, Ma P, Wei Q, Huang Y, Liu T. Hierarchically designed super-Elastic metafabric for thermal wet comfortable and antibacterial epidermal electrode. *Adv Funct Mater*. **2022**;*32*:2209762.
31. Dong Z, Liu Q, Han X, Zhang X, Wang X, Hu C, Li X, Liang J, Chen Y, Fan Y. Electrospun nanofibrous membranes of recombinant human collagen type III promote cutaneous wound healing. *J Mater Chem B*. **2023**;*11*:6346.
32. Li A, Li L, Ba Z, Li X, Liang W, Lang M, Cheng B, Li J. Antibacterial, antioxidant and anti-inflammatory PLCL/gelatin nanofiber membranes to promote wound healing. *Int J Biol Macromol*. **2022**;*194*:914.
33. Jin H, Nayeem MOG, Lee S, Matsuhisa N, Inoue D, Yokota T, Hashizume D, Someya T. Highly durable nanofiber-reinforced elastic conductors for skin-tight electronic textiles. *ACS Nano*. **2019**;*13*:7905.
34. Tan G, Xu D, Zhu Z, Zhang X, Li J. Tailoring pore size and interface of superhydrophobic nanofibrous membrane for robust scaling resistance and flux enhancement in membrane distillation. *J Membr Sci*. **2022**;*658*: 120751.
35. Wei W, Zhang P, Cao F, Liu J, Qian K, Pan D, Yao Y, Li W. Ultrathin flexible electrospun EVA nanofiber composite with electrothermally-driven shape memory effect for electromagnetic interference shielding. *Chem Eng J*. **2022**;*446*: 137135.
36. Ma P, Liang W, Huang R, Zheng B, Feng K, He W, Huang Z, Shen H, Wang H, Wu D. Super-structured wet-adhesive hydrogel with ultralow swelling, ultrahigh burst pressure tolerance, and anti-postoperative adhesion properties for tissue adhesion. *Adv Mater*. **2024**;*36*:2305400.
37. Zhang Q, Deng YX, Luo HX, Shi CY, Geise GM, Feringa BL, Tian H, Qu DH. Assembling a natural small molecule into a supramolecular network with high structural order and dynamic functions. *J Am Chem Soc*. **2019**;*141*:12804.
38. Hou Y, Guan QF, Xia J, Ling ZC, He Z, Han ZM, Yang HB, Gu P, Zhu Y, Yu SH, Wu H. Strengthening and toughening hierarchical nanocellulose via humidity-mediated interface. *ACS Nano*. **2020**;*15*:1310.
39. Zhao F, Zheng X, Zhou S, Zhou B, Xue S, Zhang Y. Constitutive model for epoxy shape memory polymer with regulable phase transition temperature. *Inter J Smart and Nano Mater*. **2021**;*12*:72.
40. Jiang X, Tian B, Xuan X, Zhou W, Zhou J, Chen Y, Lu Y, Zhang Z. Cellulose membranes as moisture-driven actuators with predetermined deformations and high load uptake. *Inter J Smart and Nano Mater*. **2021**;*12*:146.
41. Guan W, Gong C, Wu S, Cui Z, Zheng Y, Li Z, Zhu S, Liu X. Instant protection spray for anti-infection and accelerated healing of empyrosis. *Adv Mater*. **2023**;*36*:2306589.
42. Wu L, Luo Y, Wang C, Wu S, Zheng Y, Li Z, Cui Z, Liang Y, Zhu S, Shen J, Liu X. Self-driven electron transfer biomimetic enzymatic catalysis of bismuth-doped PCN-222 MOF for rapid therapy of bacteria-infected wounds. *ACS Nano*. **2023**;*17*:1448.
43. Guo Z, Zhang Z, Zhang N, Gao W, Li J, Pu Y, He B, Xie J. A Mg^{2+}/polydopamine composite hydrogel for the acceleration of infected wound healing. *Bioact Mater*. **2022**;*15*:203.
44. Wang A, Duan S, Ding X, Zhao N, Hu Y, Ding X, Xu FJ. Bioswitchable antibacterial coatings enable self-sterilization of implantable healthcare dressings. *Adv Funct Mater*. **2021**;*31*:2011165.
45. Thomason HA, Lovett JM, Spina CJ, Stephenson C, McBain AJ, Hardman MJ. Silver oxysalts promote cutaneous wound healing independent of infection. *Wound Repair Regen*. **2018**;*26*:144.
46. Ma LL, Zhou YZ, Zhang ZWB, Liu YQ, Zhai D, Zhuang H, Li Q, Yu JD, Wu CT, Chang J. Multifunctional bioactive Nd-Ca-Si glasses for fluorescence thermometry, photothermal therapy, and burn tissue repair. *Sci Adv*. **2020**;*6*:eabb1366.
47. Hong Y, Zhou F, Hua Y, Zhang X, Ni C, Pan D, Zhang Y, Jiang D, Yang L, Lin Q, Zou Y, Yu D, Arnot DE, Zou X, Zhu L, Zhang S, Ouyang H. A strongly adhesive hemostatic hydrogel for the repair of arterial and heart bleeds. *Nat Commun*. **2019**;*10*:2060.
48. Tang N, Zhang R, Zheng Y, Wang J, Khatib M, Jiang X, Zhou C, Omar R, Saliba W, Wu W, Yuan M, Cui D, Haick H. Highly efficient self-healing multifunctional dressing with antibacterial activity for sutureless wound closure and infected wound monitoring. *Adv Mater*. **2021**;*2021*:34.
49. Xi Y, Ge J, Wang M, Chen M, Niu W, Cheng W, Xue Y, Lin C, Lei B. Bioactive anti-inflammatory, antibacterial, antioxidative silicon-based nanofibrous dressing enables cutaneous tumor photothermo-chemo therapy and infection-induced wound healing. *ACS Nano*. **2020**;*14*:2904.